Polyhedron 258 (2024) 117020

Contents lists available at ScienceDirect

Polyhedron

journal homepage: www.elsevier.com/locate/poly

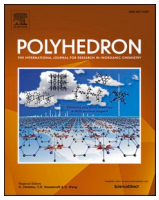

Oxidovanadium(V) complexes with tridentate hydrazone ligands as oxygen atom transfer catalysts

Md Kamal Hossain [a,b,*], Matti Haukka [c], George C. Lisensky [d], Michael G. Richmond [e], Ebbe Nordlander [a,*]

[a] Chemical Physics, Department of Chemistry, Lund University, P.O. Box 124, SE-22100 Lund, Sweden
[b] Department of Chemistry, Jahangirnagar University, Savar Dhaka-1342, Bangladesh
[c] Department of Chemistry, P.O. Box 35, University of Jyväskylä, FI-40014 Jyväskylä, Finland
[d] Department of Chemistry, Beloit College, 700 College St., Beloit, WI 53511 USA
[e] Department of Chemistry, University of North Texas, Denton, TX 76203 USA

ARTICLE INFO

Keywords:
Vanadium(V) complexes
Hydrazone ligand
^{51}V NMR
Epoxidation
Sulfoxidation
DFT

ABSTRACT

Four isostructural oxovanadium(V) complexes with hydrazone ligands have been synthesised, characterised, and evaluated as epoxidation and sulfoxidation catalysts. The reactions between $[VO(acac)_2]$ ($acac^-$ = acetylacetonate) and H_2L^n (n = 1–4), precursors for monoanionic tridentate hydrazone ligands, afford complexes formulated as $[VO(L^n)(bzh)\cdot MeOH]$ (**1**–**4**) when bidentate benzohydroxamic acid (Hbzh) is included as a co-ligand. Single crystal X-ray structure analyses showed that complexes **1**–**3** have a distorted octahedral coordination geometry with an O_5N coordination environment. Cyclic voltammetry showed that all complexes undergo two quasi-irreversible reduction peaks and a single irreversible oxidation peak. The bonding in **1** has been investigated by electronic structure calculations, and these data are discussed with respect to the electrochemical results. Complexes **1**–**4** were tested as catalysts for the epoxidation of *cis*-cyclooctene at 50 °C and sulfoxidation of methyl-*p*-tolylsulfide at room temperature using *tert*-butyl hydroperoxide (*t*BuOOH) and aqueous H_2O_2 as the terminal oxidants.

1. Introduction

Coordination complexes of vanadium have been explored for applications in many fields, e.g. as model complexes for biological sites, inhibitors of various enzymes, as reactants/catalysts in C—C bond cleavage reactions, and as oxidation catalysts [1–5]. In the area of oxidation catalysis, the catalytic potential of vanadium(IV,V) complexes in oxidation, oxidative halogenation, epoxidation and sulfoxidation of a variety of organic substrates has been studied extensively [6–10], and there is a growing interest in the latter two catalytic reactions since epoxides are key starting materials in the production of a wide variety of chemicals and fine chemicals while sulfoxides and sulfones are of considerable importance in medicinal chemistry [11–13]. We have previously reported oxovanadium(V) complexes carrying amino bisphenolate ligands with different nitrogen side-arm donors as active catalysts for epoxidation, sulfoxidation and haloperoxidation reactions [14–18]. Relative to other oxovanadium(V) complexes, only a small number of Schiff base oxovanadium(V) complexes have been investigated for their abilities to catalyse epoxidation and sulfoxidation reactions [19–25].

Among various ligand systems, hydrazide and hydrazone compounds possess excellent characteristics for coordination to transition metals *via* O, N and S coordinating environments, *e.g.* NNO or NNS donor sets [26–28]. Numerous oxovanadium complexes with a variety of hydrazone ligands have been prepared for their insulin mimetic properties [29–31]. Some binuclear vanadium(IV) complexes containing ligands based on Schiff base derivatives of hydrazones have been studied for urease inhibitory activities [32,33]. Several groups have previously examined the cytotoxic and antimicrobial activities as well as the electrochemical properties of oxovanadium hydrazone complexes, especially such complexes containing VO^{2+}, VO^{3+} and $V_2O_3^{4+}$ motifs [34–38].

Here we present the syntheses, spectroscopic characterization, and crystal structure determinations of four new oxovanadium complexes containing the tridentate hydrazone ligands L^n (n = 1–4, Fig. 1). These ONO'-donor ligands, previously reported by Lei *et al.* and Shakira *et al.*

* Corresponding authors at: Chemical Physics, Department of Chemistry, Lund University, P.O. Box 124, SE-22100 Lund, Sweden.
E-mail addresses: k_hossain_ju@yahoo.com (M.K. Hossain), ebbe.nordlander@chemphys.lu.se (E. Nordlander).

https://doi.org/10.1016/j.poly.2024.117020
Received 27 December 2023; Accepted 2 May 2024
Available online 3 May 2024

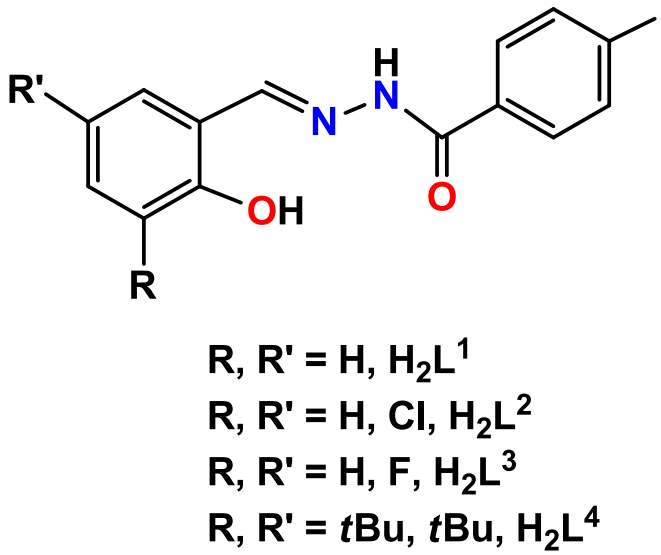

Fig. 1. Pro-ligands H_2L^n (n = 1–4) used in this study [58].

[58], contain a phenolate moiety that may allow tuning of the electronic properties of the donor atom(s) by judicious choice of electron-withdrawing or electron-donating groups located in the *para* position of the phenolate donor. In addition to the parent structure (L^1), this set of ligands contains two electron-withdrawing substituents (Cl, F; L^2 and L^3, respectively) and one electron-donating substituent (^{t}Bu, L^4) in *para* position. In the present study, we have examined catalytic epoxidation and sulfoxidation reactions of the four vanadium complexes with *tert*-butyl hydroperoxide (^{t}BuOOH) and aqueous H_2O_2 as the ultimate oxidants.

2. Results and discussion

2.1. Syntheses and spectroscopic characterization of complexes

Solutions of $[VO(acac)_2]$, hydrazone pro-ligands H_2L^n (n = 1–4) and benzohydroxamic acid in methanol were stirred for 2 h at room temperature to prepare complexes **1**–**4** (Scheme 1). All compounds were crystallized as black or dark red crystals from concentrated reaction mixtures by slow evaporation of the solvent at room temperature. All complexes are soluble in DMF, DMSO, methanol, ethanol, chloroform and acetonitrile. The new products are stable in the solid state and in solution at room temperature for several months.

The complexes were characterized by a variety of spectroscopic techniques (IR, ^{1}H, ^{13}C{^{1}H}, ^{51}V NMR, ESI-MS) in combination with X-ray crystallography. The IR spectra show strong stretches at 972, 962, 970 and 975 cm^{-1}, for **1**, **2**, **3** and **4**, respectively, which are readily attributed to the ν(V = O) stretching band. The observed ν(V = O) resonances for **1**–**4** may be compared to structurally similar vanadium(V) oxido hydroxamate complexes with similar donor sets and coordination spheres. For example, the complexes $[VO(aha)(L^{n'})]$ (n = 1–4; Haha = acetohydroxamic acid, $H_2L^{1'}$ = 4-nitrophenyl 2-(2-hydroxybenzylidene) hydrazinecarboxylate, $H_2L^{2'}$ = N′-(2-hydroxylbenzylidene)-4-methoxybenzohydrazide, $H_2L^{3'}$ = N′-(2-hydroxylbenzylidene)-4-methylbenzohydrazide, $HL^{4'}$ = N′-(5-bromo-2-hydroxy-benzylidene)-3-methyl benzohydrazide) exhibit ν(V = O) stretching frequencies of 973, 955, 966 and 971 cm^{-1}, respectively. Other examples include the two benzohydroxamate complexes $[VO(L^{n''})(L'')]$ (n = 1, 2; $L^{1''}$ = the dianionic form of N′-(3,5-dibromo-2-hydroxybenzylidene)-4-methoxybenzohydrazide, $L^{2''}$ = N′-(3,5-dibromo-2-hydroxybenzylidene)nicotinohydrazide, L″ = benzohydroxamate) that are closely similar to **1**–**4** and for which ν(V = O) appears at 978 and 973 cm^{-1}, respectively, which can also be compared with our synthesized complexes [15,39–41]. A comparison of ν(V = O) frequencies and ^{51}V NMR data for **1**–**4** with those of a number of related complexes are found in Table S1 (Supplementary Information).

The ^{1}H, ^{13}C, and ^{51}V NMR spectra were measured in $CDCl_3$ or CD_3CN (see supplementary material for the full ^{51}V NMR spectra). The disappearance of the chemical shifts of phenolic OH protons in the complexes suggests deprotonation and coordination of the phenolic oxygen moiety of the corresponding salicylaldehyde to vanadium. Furthermore, the disappearance of the ^{1}H NMR resonance assigned to the amide (–CONH–) proton indicates that this group is also involved in the bonding to the vanadium ion through the O donor via enolisation followed by deprotonation, which is evident from the X-ray structures of **1**–**3** (*vide infra*). The aromatic protons of all compounds are observed in the region δ 6.92–8.85 ppm. The ^{13}C NMR spectra show the aromatic carbons in the δ 116–171 ppm range (*cf.* Experimental Section for details).

The ^{51}V NMR spectra of the new V(V) complexes consist of a single sharp singlet in each case, resonating at ca. −434 ppm (**1**), −447 ppm (**2**), −448 ppm (**3**) and −461 ppm (**4**), respectively (see Figure S1). The electrospray ionization (ESI) mass spectral analyses of **1**–**4** were recorded in acetonitrile solution and reveal a molecular ion peak corresponding to the metal complex $[M + MeOH]^+$ for each complex. Peaks for the corresponding protonated complex $[M + H]^+$ and MeCN-solvated complex $[M + MeCN]^+$ were also observed for all compounds. Moreover, we have also taken high-resolution mass spectrometry (HRMS) of the studied all complexes that precisely matches with a molecular ion peak (see experimental section). All mass spectra were found to exhibit isotopic distributions consistent with the expected isotopic composition.

2.2. Molecular structures of complexes 1–3

Crystals of complexes **1**, **2** and **3** were obtained by slow evaporation from concentrated methanol solutions at room temperature and their structures were determined by single crystal X-ray diffraction analysis.

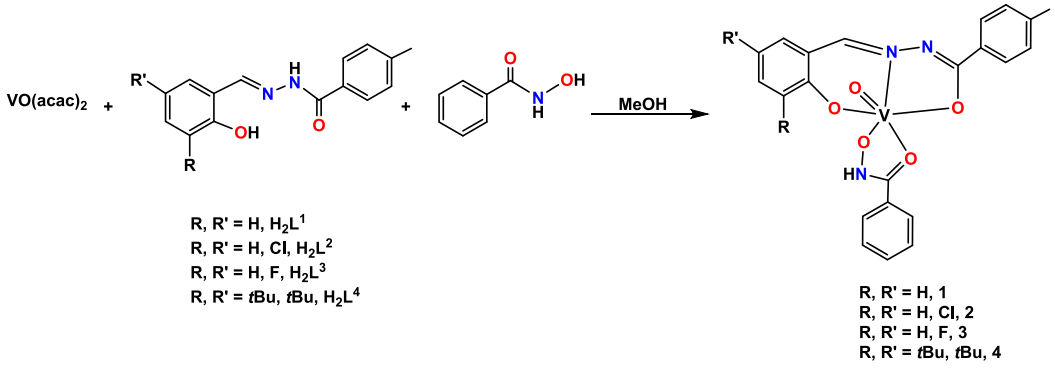

Scheme 1. Formation of the mononuclear V(V) complexes **1**–**4** investigated in this work.

Relevant crystallographic data for **1**–**3** and selected bond lengths and angles are listed in the supplementary material (Tables S2 and S3). The molecular structures of **1**–**3** are shown in Figs. 2-4. The solid-state structures confirm that **1**–**3** are mononuclear vanadium complexes where the six-coordinate vanadium(V) ion exhibits a slightly distorted octahedral geometry.

The monoanionic tridentate hydrazone ligand and benzohydroxamate ion coordinate to the V atom through the phenolate O, imine N and enolic O atom of the deprotonated ligands $(L^n)^{2-}$ as well as the alcohol and ketone oxygens of the benzohydroxamate moiety, generating one six- and two five-membered chelate rings. Several configurational isomers of the complexes are possible, but the three crystal structures show only one (chiral) configurational isomer– a meridional isomer with the hydrazone ligand being almost planar and the keto oxygen of the hydroxamate ligand being coordinated *trans* to the oxido ion of the V(V) = O unit (*cf.* Scheme 1 and Figs. 2-4), that is found as a racemic mixture of two possible enantiomers.

The bite angles of the hydrazine-based six- and five-membered rings are 83.70(8)° and 75.03(8)° for **1,** 83.88(7)° and 75.16(7)° for **2**, and 75.24(7)° and 83.76(7)° for **3**. The distorted NO_5 octahedral coordination with the O,N,O donor atoms of the hydrazone ligand and the benzohydroxamate O atom define the equatorial plane whereas the oxido ketone oxygens occupy axial positions with an O5-V1-O4 angle of 168.43(9)°. The C—O, C—N and N—N distances are consistent with related five-membered chelate rings containing the enolate moiety in other published hydrazone complexes [42–44].

The five V–O bond distances in the studied compounds are unequal and follow the usual order, *i.e.* V–O(oxido) < V–O(alkoxide) < V–O (phenoxide) < V–O(enolate) < V–O(keto), which are consistent with the π-bonding strength and the basicity exerted by the O-donor moieties of both the ligand and co-ligand. The V–O bond lengths are approximately 1.90 Å for the phenolate oxygen atoms. Typical V = O double bond distances of approximately 1.60 Å are observed for complexes **1**–**3**, which are within the range found for similar complexes [35,37,45].

The average vanadium-amide (keto) oxygen bond distances, V(1)-O (4), are around 2.22 Å, which is longer than the average vanadium-hydroxamate oxygen bond distances of the coordinated benzohydroxamates, V(1)-O(3), (approx. 1.88 Å) for all comparable complexes. These distances are in agreement with the N—O oxygen formally coordinating as an anionic donor, while the C═O oxygen coordinates as a neutral donor. Both the coordinated oxido anion and the anionic N—O donor entity exert a structural *trans* influence. The carbonyl oxygen O(4) of the benzohydroxamate co-ligand is *trans* to the terminal oxido O(5) atom, rendering the C═O group weakly bonded to the vanadium center. The approx. 2.085 Å bond length of V(1)-N(2) is also lengthened due to N(2) being *trans* to the coordinated N—O group.

In the crystal structures of complexes **1** and **3**, there is an intermolecular hydrogen bond between the phenolate moiety of the hydrazone ligand and a methanol solvent molecule, O2···H6-O6 (approx. 1.9 Å), while in complex **2** there is a longer intermolecular hydrogen bond between the vanadium oxido ion and a methanol molecule, O5···H6-O6 (approx. 2.17 Å) (Figs. 1-3). The phenolate C—O bond distances are not significantly affected by the nature of the *para*-substituent; the C(15)-O (2) distance is approx. 1.35 Å for complexes **1** and **3** and the corresponding C(1)-O(1) distance is approx. 1.33 Å for complex **2**. There is a very slight elongation of the V-O bond *trans* to the coordinated phenolate for complex **3** (V(1)-O(1) = 1.9535(16) Å, relative to the corresponding distances for **1** (V(1)-O(1) = 1.9729(18) Å) and **2** (V(1)-O(2) = 1.9183(16) Å.

2.3. Electrochemical studies

The vanadium complexes **1**–**4** were studied by cyclic voltammetry (CV) under a nitrogen atmosphere. Important features are summarized in Table 1 and the cyclic voltammograms are provided in the Supporting Information, see Figs. S2-S5. On scanning towards a more negative potential, two quasi-irreversible reductions take place, presumed to be the V(V) to V(IV) and the V(IV) to V(III) reductions. The reversibility does

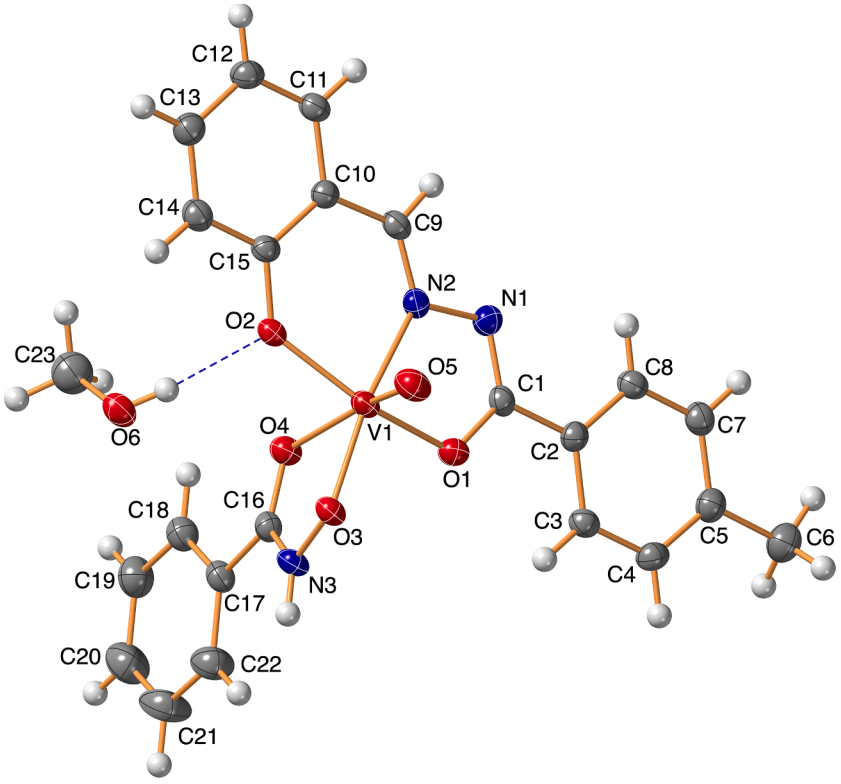

Fig. 2. The solid-state structure of **1**, containing a hydrogen-bonded methanol molecule (O6-O2 = 1.93 Å). Thermal ellipsoids are drawn at the 50 % probability level.

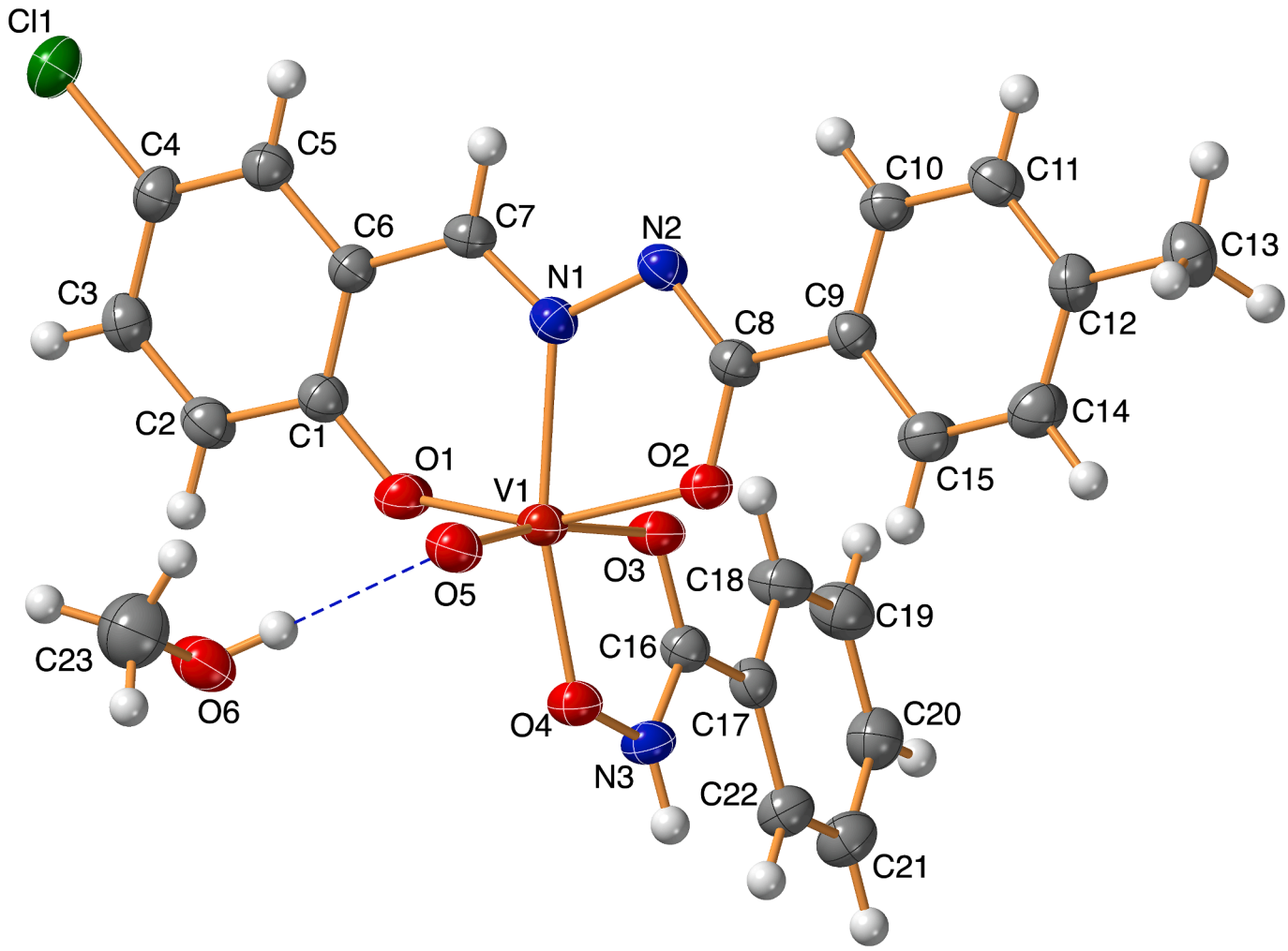

Fig. 3. The solid-state structure of **2**, containing a hydrogen-bonded methanol molecule (O6-O5 = 2.17 Å) Thermal ellipsoids are drawn at the 50 % probability level.

not improve with increasing scan rate, even at 4 V/s, so the lack of reversibility does not indicate chemical decomposition. The $E_{1/2}$ values for **1**–**4** shift to more positive values with the addition of electron-withdrawing groups and to more negative values with the addition of electron-donating groups, as quantified by the Hammett parameter for *para* substituents σ^p (H = 0; Cl = +0.227; F = +0.062; tBu = -0.2, see Fig. 5) [46]. On scanning towards a more positive potential, a quasi-reversible oxidation takes place, which is presumably an oxidation of the ligand as a metal-centered oxidation may be ruled out (see also computational modelling, below). The observed redox potentials are similar to those reported earlier for related vanadium(V) complexes [6,47–49] (*cf.* Table S4). However, we did not find the $E_{1/2}$ values to be predictive of the oxygen atom transfer activities of the different complexes.

Computational modelling was used to assess the nature and the location of charge in both the reduced and oxidized forms of the vanadium oxido complexes. The nature of the HOMO and LUMO in complex **1** was investigated by DFT calculations. The optimized structure of the neutral species **A** appears in Fig. 6. Excellent agreement between **A** and the experimental structure (Fig. 2) is noted. The contour plots of the HOMO and LUMO levels for **A** are depicted alongside the optimized structure, and these frontier orbitals serve as the sites for the initial oxidation and reduction processes. The orbital plot of the HOMO confirms its parentage as a ligand-based orbital that involves the π system of the tridentate O,O,N ligand. The LUMO is best described as a metal-based d_{xy} orbital that is surrounded by five out-of-phase π interactions from the oxygen atoms that comprise the octahedral VO_5N core.

The structures of the radical cation ($^2\mathbf{A}^1$) and radical anion ($^2\mathbf{A}^{1-}$) were also optimized (not shown) in order to study the primary oxidation and reduction products [50]. Both radical species exhibited only minor structural differences compared with **A**, supporting the fact that HOMO and LUMO levels in **A** serve as the highest singularly occupied molecular orbital (SOMO) upon one-electron oxidation and one-electron reduction of **A**. The spin density plots for the radical cation ($^2\mathbf{A}^1$) and radical anion ($^2\mathbf{A}^{1-}$) species are shown in Fig. 7, where the spin density on the radical cation is localized over the tridentate O,O,N ligand and the spin density on the radical anion is confined to the vanadium atom and the surrounding oxygen periphery. These data are in concert with the observed electrochemical trends.

3. Catalysis studies

3.1. Catalytic epoxidation

As expected, all four V complexes showed catalytic activity for the benchmark reaction of epoxidation of *cis*-cyclooctene, using three equivalents of *tert*-butylhydroperoxide (TBHP, 5.5 M in decane) as an oxidant in $CDCl_3$ (Scheme 2), albeit with different activities (results are summarized in Table 2). Products were identified by ^{1}H NMR spectroscopy. Control experiments in the absence of catalysts gave no epoxide products. There was no epoxide formed at room temperature but at 50 °C all complexes reached some activity after approximately two hours. The presence of a strong electron withdrawing substituent, like fluorine in complex **3**, resulted in the highest catalytic activity,

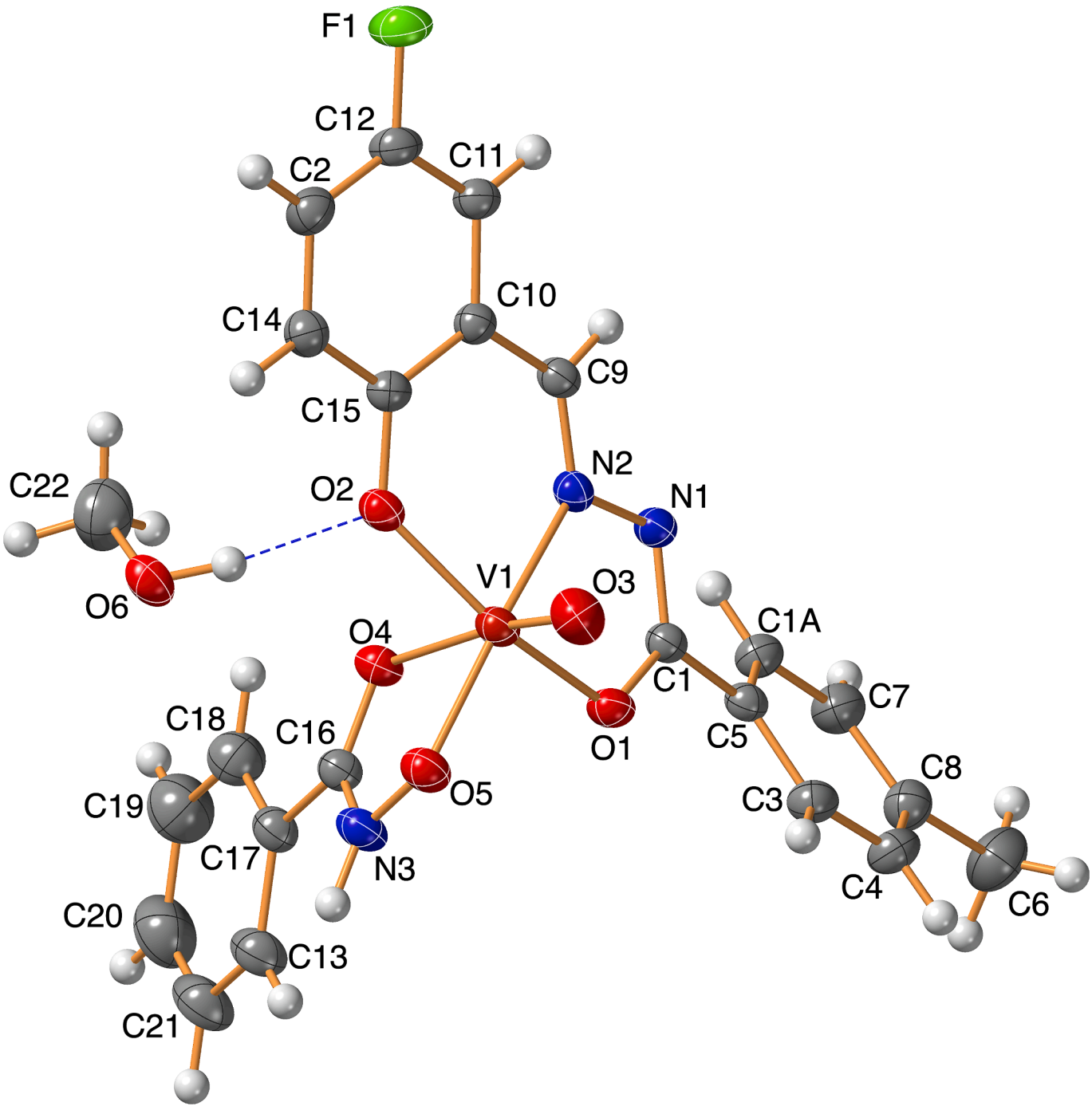

Fig. 4. The solid-state structure of **3**, containing a hydrogen-bonded methanol molecule (O6-O2 = 1.86 Å). Thermal ellipsoids are drawn at the 50 % probability level.

reaching a yield of 95 % after 3 h in the epoxidation of *cis*-cyclooctene while the other three complexes (**1**, **2** and **4**) gave good yields of epoxide (>95 %) after 8 h for **1** and **2** and 24 h for **4**. The reactivity of these latter three catalysts exhibited almost the same profile. The epoxidation activities of **1**–**4** are comparable with those found for the vanadium(V) complexes [VO(L^1)(OMe)], [VO(L^2)(acac)], and [VO(L^3)] (H_2L^1 = 6,6′-(((2-morpholinoethyl)azanediyl)bis(methylene))bis(2,4-di-*tert*-butylphenol), H_2L^2 = 6,6′-(((thiophen-2-ylmethyl)azanediyl)bis(methylene))bis(2,4-di-*tert*-butylphenol); H_3L^3 = 2,2′-((3,5-di-*tert*-butyl-2-hydroxybenzyl)azanediyl)bis(ethan-1-ol) as well as [VO(L^2)] and [VO(L^3)] (L^2 is tripodal 2-propanolamine bisphenolate; L^3 is pentadentate ethoxyethanolamine bisphenolate) [6,15]. During the catalytic reactions, the stabilities of the complexes toward alkyl hydroperoxides were checked. It was observed that the colour of the reaction mixture changed from red to yellow during the reactions. After 24 h, all vanadium catalysts showed five distinct signals in ^{51}V NMR (^{51}V ≈ −539, −589, −657, −658, −672 ppm, see supporting material, Figures S6 and S7) corresponding to five different species, indicating slow decomposition during the catalytic process. The natures of these decomposition products have not been elucidated. The appearance of multiple ^{51}V NMR signals after 24 h in $CDCl_3$ or 16 h in CD_3CN suggests that the original (catalyst precursor) complexes or even the presumed catalytically active peroxide species are possibly not the only species in solution that can drive the oxidation reactions forward.

Table 1
Oxidation and reduction potentials $E_{1/2}$ [V] vs. Fc^+/Fc of **1**–**4** obtained from cyclic voltammograms in MeCN solution.

complex	potential ($E_{1/2}$) of first reduction peak (V)	potential ($E_{1/2}$) of second reduction peak (V)	potential ($E_{1/2}$) of first oxidation peak (V)
[VO(L^1)(bzh)·MeOH] (**1**)	−0.453	−1.177	−0.023
[VO(L^2)(bzh)·MeOH] (**2**)	−0.413	−1.136	0.024
[VO(L^3)(bzh)·MeOH] (**3**)	−0.438	−1.268	−0.005
[VO(L^4)(bzh)·MeOH] (**4**)	−0.588	−1.370	−0.178

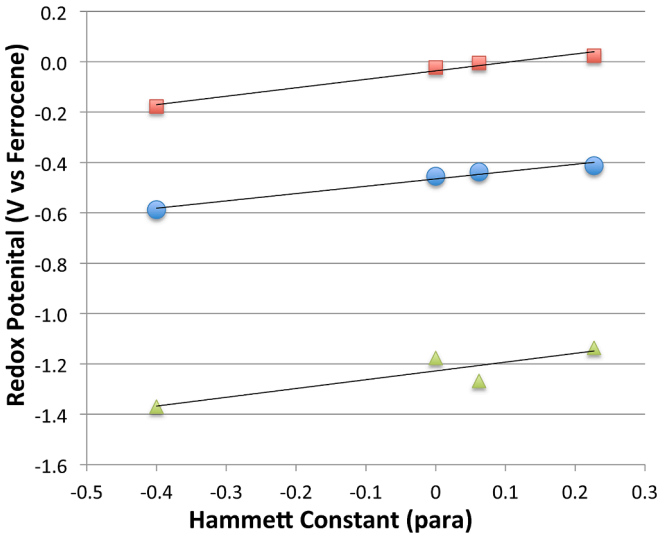

Fig. 5. Correlation of oxidation and reduction potentials of **1**–**4** with Hammett parameter σ^p. Circles: first reduction, correlation 0.98; triangles: second reduction, correlation 0.80; squares: first oxidation, correlation 0.98. Both *o,p*-substituents are counted for complex **4**.

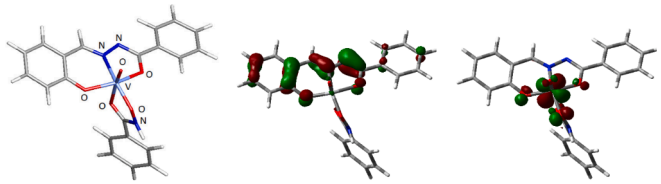

Fig. 6. DFT data on species **A**. The geometry-optimized structure of **A** appears to the left. The center contour plot shows the HOMO ($^2\mathbf{A}^1$) and the LUMO ($^2\mathbf{A}^{1-}$) appears to the right. The orbital pictures are printed at an isovalue of 0.055.

In order to improve the reaction rate, the epoxidation of cyclooctene catalysed by complex **1** was studied in CD_3CN solution at 75° C. However, this reaction resulted in a reduction in yield of the epoxide product by *ca*. 30 % after 8 h. This decrease in activity is presumably due to decomposition of the oxidant and/or catalyst at the elevated temperature [14], probably due to the formation of oxygen-bridged dimeric species or decomposition to simple inorganic vanadates.

Unfortunately, the new vanadium complexes did not show any activity when epoxidations were performed in aqueous H_2O_2 instead of ^{t}BuOOH. This is in agreement with previous studies on oxidation reactions catalysed by vanadium oxido complexes, where it was observe that when the reactions were run in aqueous H_2O_2 as an oxidant, the epoxidation activity was very low and the oxidant seemed to decompose during the reaction [51–53].

3.2. Catalytic sulfoxidation

Complexes **1**–**4** were also tested as catalysts for sulfoxidation of methyl-*p*-tolylsulfide with three equivalents of ^{t}BuOOH and H_2O_2 (35 % in water) as oxidants (Scheme 3). The reactions were run in $CDCl_3$ solution and were monitored ^{1}H NMR, with the temperature maintained at 25 °C by thermostatic control. It was found that complexes **1**–**4** were capable of activating *t*BuOOH or H_2O_2 and oxidizing methyl-*p*-tolylsulfide to the corresponding sulfoxide. However, the solubility of aqueous H_2O_2 in $CDCl_3$ solution is lower than for *t*BuOOH, and the catalytic reactions with hydrogen peroxide were found to be slower than those employing *t*BuOOH as oxidant. Control experiments carried out in the absence of catalyst gave no reaction. Conversely, the catalytic reactions started immediately without any noticeable induction times. The sulfoxidation results are compiled in Table 3.

From the observations with ^{t}BuOOH and aqueous H_2O_2, it can be concluded that the three complexes **1**, **2** and **4** showed similar catalytic activities in sulfoxidation reactions using both oxidants; conversion of methyl-*p*-tolylsulfide to the corresponding sulfoxide is quantitative (>98 %). Interestingly, the fluorine-substituted complex **3** was again found to be the best catalyst. It exhibited excellent activity; the reactions were much faster than for the other three catalysts, reaching 98 % yield of sulfoxide after half an hour when ^{t}BuOOH was used as oxidant. Significantly lower activity was observed with **3** when sulfoxidation was performed with H_2O_2 instead of ^{t}BuOOH, reaching 99 % yield of sulfoxide after 20 h. All complexes showed one extra peak in the ^{51}V NMR spectrum after 24 h in ^{t}BuOOH solutions (^{51}V ≈ −448, −600 ppm (extra peak), see supporting material, Fig. S7) which indicates that the catalysts are not stable under turnover conditions. On the other hand, the complexes appeared to be stable in the presence of H_2O_2 solutions and no extra peaks were observed in the ^{51}V NMR spectra after the completed reactions. Only trace amount of sulfone was observed. Possible enantioselectivity in the sulfoxidation reactions was not evaluated for this study. The yields of sulfoxide were good and comparable with those observed for vanadium diaminebis(phenolate) complexes and our previously published oxovanadium(V) complexes with tripodal bisphenolate and monophenolate ligands [15,17,51–53].

4. Summary and conclusions

The vanadium(V) oxo complexes [VO(L^n)(bzh)] (n = 1–4) were readily obtained by reaction of the V(IV) complex [VO(acac)$_2$] with the ligand precursors HL^n in the presence of benzohydroxamic acid. Single crystal X-ray structure analyses of three of the complexes reveal distorted octahedral O_5N coordination environments around the V(V) ions. Complexes **1**–**4** are capable of effecting catalytic oxidations of *cis*-cyclooctene and methyl-*p*-tolylsulfide using *tert*-butyl hydroperoxide or aqueous H_2O_2 as oxidants. All vanadium complexes could catalyse the oxidation of *cis*-cyclooctene to its epoxide in more than 95 % yield using *tert*-BuOOH as oxidant. It was also found that **1**–**4** are effective catalysts in the sulfoxidation reaction, giving better than 98 % yields with both oxidants and chloroform as solvent. No direct correlation could be made between the Hammett parameter for *para*-substituents of the phenolate parts of the hydrazone ligands and the catalytic activity of the complexes. We hypothesize that the relative lack of influence of the electronic property of the hydrazone ligand may be connected with the formation of an active vanadium peroxide catalyst complex where the peroxo moiety is located in an axial position rather than the equatorial plane where the hydrazone ligand is found. Nevertheless, complex **3**, with fluorine in the *para* position of the coordinated phenolate unit, is clearly the best catalyst for both reactions probed in the present study.

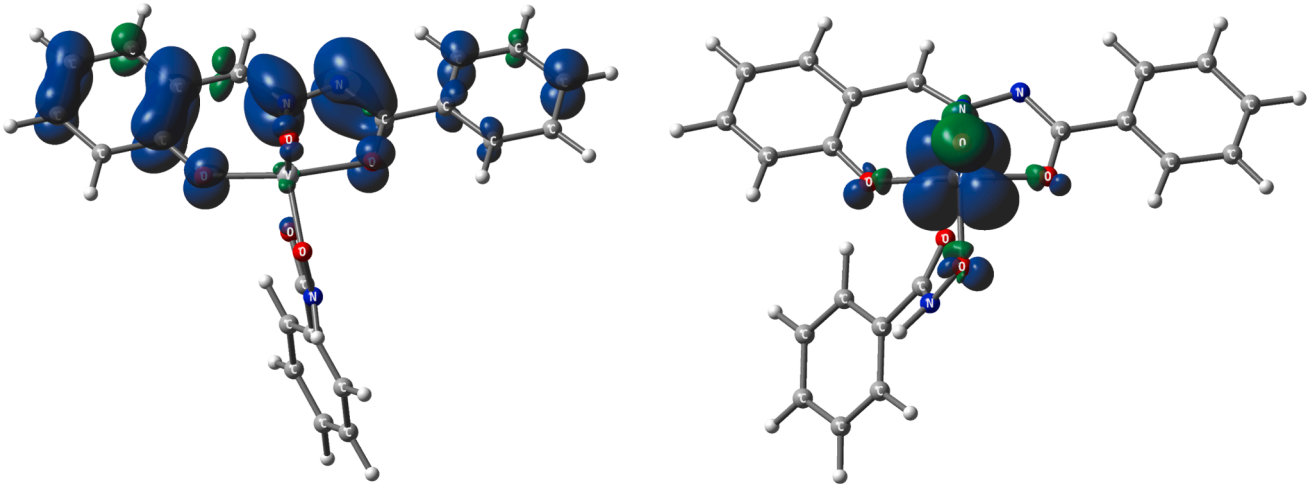

Fig. 7. Spin density plots of the radical cation $^{2}\mathbf{A}^{1}$ (left) and the radical anion $^{2}\mathbf{A}^{1-}$ (right). The isovalue for each α-spin based contour plot is 0.055.

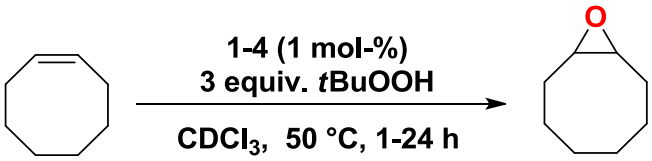

Scheme 2.

Table 2
Epoxidation of *cis*-cyclooctene by *tert*-BuOOH.

1		2		3		4	
Yield	t	Yield	t	Yield	t	Yield	t
[%]	[h]	[%]	[h]	[%]	[h]	[%]	[h]
>95	8	>95	8	>95	3	>95	24

Reaction conditions: Yield of the product measured by ^{1}H NMR. 1 mol-% of catalyst (**1**–**4**), 3.0 equivalents of *tert*-BuOOH at 50 °C.

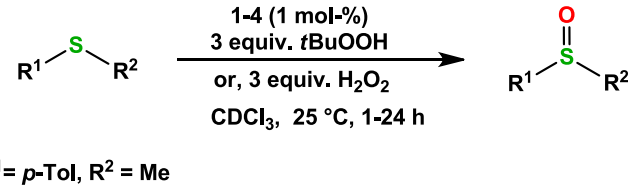

Scheme 3.

Table 3
Sulfoxidation of methyl-*p*-tolylsulfide at 25 °C.

	1		2		3		4	
	Yield [%]	T [h]	Yield [%]	t [h]	Yield [%]	t [h]	Yield [%]	t [h]
*t*BuOOH	>98	24	>99	6	>98	0.5	65	24
H_2O_2	>98	24	>98	24	>99	20	90	24

Reaction conditions: Yield of the product as measured by ^{1}H NMR. 1 mol-% of catalyst (**1**–**4**), 3.0 equivalents of ^{t}BuOOH and H_2O_2 (35 % in water) at 25 °C.

However, none of the catalysts were found to be stable under prolonged catalytic reactions under the reaction conditions employed. Further studies might probe any electronic influence of the hydroxamate ligand on catalyst activity.

5. Experimental section

5.1. Materials and physical measurements

Commercial grade chemicals were used without further purification for synthetic purposes and HPLC grade solvents were used as purchased. All syntheses and manipulations were performed under ambient laboratory atmosphere. The ^{1}H, ^{13}C and ^{51}V NMR spectra were recorded using a Varian Inova 500 MHz spectrometer (^{1}H: 500.13 MHz, ^{13}C: 125.76 MHz, ^{51}V: 131.55 MHz) in $CDCl_3$ or CD_3CN solutions at room temperature, and referenced to the residual signal of the solvent in the case of the ^{1}H and ^{13}C spectra. The ^{51}V chemical shifts are reported in ppm from the TMS ^{1}H frequency ($\delta = 0$ ppm), using $VOCl_3$ as external standard. The 1D ^{51}V NMR spectra were measured with a single pulse-acquire sequence (pulse angle 90° and acquisition delays 0.3 s). Infrared spectra were recorded on a Bruker Optics ALPHA FT-IR spectrometer in the Centre for Analysis and Synthesis at Lund University. Electrospray ionization (ESI) mass spectra were measured with a Waters ZQ 4000 spectrometer using CsI as a calibrant. In addition, high-resolution mass spectrometry (HRMS) was performed on Waters QTof Xevo-G2 spectrometer and the samples were injected as MeCN with traces of water. Results are denoted as cationic mass peaks; unit is the mass/charge ratio.

5.2. Crystallography

The crystals of **1**–**3** were immersed in cryo-oil, mounted in a loop, and measured at a temperature of 170 K. The X-ray diffraction data were collected on a Bruker Kappa Apex II diffractometer using Mo Kα radiation. The *Denzo-Scalepack* [54] software package was used for cell refinements and data reductions. An empirical multi-scan absorption correction based of equivalent reflections (*SADABS*) [55] was applied to the intensities before structure solutions. The structures were solved by charge flipping method using the *SUPERFLIP* [56] software. Structural refinements were carried out using *SHELXL* [57] software. In **1** and **3** the NH and OH hydrogen atoms were located from the difference Fourier map but constrained to ride on their parent atom with $U_{iso} = 1.5\ U_{eq}$(-parent atom). Other hydrogen atoms were positioned geometrically and constrained to ride on their parent atoms, with C—H = 0.95–0.98 Å, N—H = 0.88 Å, O—H = 0.84 Å, and $U_{iso} = 1.2$–$1.5\ U_{eq}$(parent atom).

5.3. Preparation of the ligands

The hydrazone ligands H_2L^n (n = 1–4) [58] were prepared by reacting equimolar amounts of the respective salicylaldehyde (10 mmol) with *p*-toluic hydrazide (10 mmol) in methanol (50 mL). All spectroscopic measurements were found to match perfectly with the reported data for these ligands [58].

5.4. Syntheses of complexes 1–4

General procedure: $[VO(acac)_2]$ (1.0 mmol) was dissolved in methanol and equimolar quantities (1.0 mmol) of the respective ligand (H_2L^n) and benzohydroxamic acid (1.0 mmol) dissolved in the same solvent were added to the solution at room temperature for 2 h to give a deep red solution. The resulting dark red solution was kept for three days leading to the formation of well-shaped red single crystals by slow evaporation at room temperature. Transparent needle or block-like red crystals suitable for X-ray analysis were filtered off, washed three times with cold hexane and dried in air in good (68–80 %) yields.

$[VO(L^1)(bzh)]$ **1**, red crystals, 0.37 g (80 %). ^{1}H NMR (500 MHz, $CDCl_3$) δ 8.85 (s, 1H), 7.91 (d, J = 8.1 Hz, 2H), 7.73 (d, J = 8.1 Hz, 2H), 7.59 – 7.47 (m, 3H), 7.38 (t, J = 8.1 Hz, 2H), 7.19 (d, J = 8.1 Hz, 2H), 6.99 (dd, J = 13.7, 8.0 Hz, 2H), 2.38 (s, 3H), 2.02 (s, 1H). ^{13}C NMR (126 MHz, $CDCl_3$) δ 168.01, 165.36, 154.18, 142.18, 135.14, 133.25, 132.37, 129.13, 129.02, 128.84, 127.52, 127.13, 120.75, 119.60, 116.39 (Ar-C), 21.55 (CH_3). ^{51}V NMR (131 MHz, $CDCl_3$) δ −433.67. Selected FT-IR (cm^{-1}): 972 s (V = O). ESI-MS: m/z = 497 $[VO(L^1)(bzh) + MeCN]^+$, 488 $[VO(L^1)(bzh)\cdot MeOH + H]^+$, 456 $[VO(L^1)(bzh) + H]^+$. HRMS: m/z = 456.0756 $[VO(L^1)(bzh) + H]^+$.

$[VO(L^2)(bzh)]$ **2**, black crystals, 0.42 g (85 %). ^{1}H NMR (500 MHz, $CDCl_3$) δ 8.77 (s, 1H), 7.91 (d, J = 8.1 Hz, 2H), 7.73 (d, J = 8.1 Hz, 2H), 7.50 (d, J = 8.1 Hz, 2H), 7.45 – 7.33 (m, 3H), 7.19 (d, J = 8.1 Hz, 2H), 6.92 (d, J = 8.1 Hz, 1H), 3.50 (s, 3H), 2.38 (s, 3H). ^{13}C NMR (126 MHz, $CDCl_3$) δ 168.98, 165.52, 152.73, 142.25, 134.64, 133.49, 130.81, 129.25, 129.22, 128.96, 127.63, 127.09, 125.14, 120.76, 118.19 (Ar-C), 51.02 (*Me*OH), 21.73 (CH_3). ^{51}V NMR (131 MHz, $CDCl_3$) δ −446.53. Selected FT-IR (cm^{-1}): 962 s (V = O). ESI-MS: m/z = 530 $[VO(L^2)(bzh) + MeCN]^+$, 522 $[VO(L^2)(bzh)\cdot MeOH + H]^+$, 490 $[VO(L^2)(bzh) + H]^+$. HRMS: m/z = 490.0387 $[VO(L^2)(bzh) + H]^+$.

$[VO(L^3)(bzh)]$ **3**, black crystals, 0.40 g (83 %). ^{1}H NMR (500 MHz, $CDCl_3$) δ 8.78 (s, 1H), 7.91 (d, J = 8.1 Hz, 2H), 7.72 (d, J = 8.1 Hz, 2H), 7.53 (t, J = 7.7 Hz, 1H), 7.40 (t, J = 7.7 Hz, 2H), 7.21 (dd, J = 16.7, 8.1 Hz, 4H), 6.94 (dd, J = 8.5, 4.3 Hz, 1H), 2.38 (s, 3H). ^{13}C NMR (126 MHz, $CDCl_3$) δ 171.76, 165.43, 161.05, 157.25, 155.35, 152.88, 133.25, 129.13, 128.99, 127.52, 127.07, 122.26, 122.07, 117.63, 117.57 (Ar-C), 21.60 (CH_3). ^{51}V NMR (131 MHz, $CDCl_3$) δ −447.69. Selected FT-IR (cm^{-1}): 970 s (V = O). ESI-MS: m/z = 538 $[VO(L^3)(bzh) + MeCN + Na]^+$, 514 $[VO(L^3)(bzh) + MeCN]^+$, 496 $[VO(L^3)(bzh) + Na]^+$, 474 $[VO(L^3)(bzh) + H]^+$. HRMS: m/z = 496.0493 $[VO(L^3)(bzh) + Na]^+$, 474.0670 $[VO(L^3)(bzh) + H]^+$.

$[VO(L^4)(bzh)]$ **4**, black crystals, 0.41 g (73 %). ^{1}H NMR (500 MHz, $CDCl_3$) δ 8.80 (s, 1H), 7.93 (d, J = 8.0 Hz, 2H), 7.69 (d, J = 7.7 Hz, 2H), 7.58 (s, 1H), 7.51 (t, J = 7.4 Hz, 1H), 7.39 (t, J = 7.6 Hz, 2H), 7.35 (s, 1H), 7.18 (d, J = 7.9 Hz, 2H), 2.38 (s, 3H), 1.41 (s, 9H), 1.36 (s, 9H). ^{13}C NMR (126 MHz, $CDCl_3$) δ 170.59, 165.06, 161.77, 154.83, 143.19, 141.51, 136.07, 132.94, 130.11, 128.99, 128.93, 128.75, 127.33, 126.47, 119.06 (Ar-C), 35.25, 34.33 ($C(CH_3)_3$), 31.37, 29.60 (CH_3), 21.09 (CH_3). ^{51}V NMR (131 MHz, $CDCl_3$) δ −460.14. Selected FT-IR (cm^{-1}): 975 s (V = O). ESI-MS: m/z = 631 $[VO(L^4)(bzh) + MeCN + Na]^+$, 608 $[VO(L^4)(bzh) + MeCN]^+$, 590 $[VO(L^4)(bzh) + Na]^+$, 568 $[VO(L^4)(bzh) + H]^+$. HRMS: m/z = 590.1826 $[VO(L^4)(bzh) + Na]^+$, 568.2004 $[VO(L^4)(bzh) + H]^+$.

5.5. Typical procedure for epoxidation

The catalytic epoxidation of *cis*-cyclooctene was studied in deuterated chloroform solutions employing *tert*-BuOOH as the terminal oxidant. The catalyst, substrate and oxidant were used in a ratio of 1:100:300 with concentrations of 0.002 M, 0.2 M and 0.6 M respectively. The reaction progress was monitored and analyzed by ^{1}H NMR and 1,2-dichloroethane was used as an internal standard. Epoxide was the major product as the alkene multiplet (5.6 ppm) converts to the epoxide multiplet (2.9 ppm). The initial red or black (dark) solutions turned completely yellow after completion of the reaction.

5.6. Typical procedure for sulfoxidation

Reactions were carried out at room temperature in deuterated chloroform solutions using a 1:3 M ratios of substrate/*t*BuOOH (0.2 M: 0.6 M) and added 10 μL of 1,2-dichloroethene as an internal standard in a 5 mm NMR tube. The reactions were monitored by ^{1}H NMR spectroscopy using a fifteen-minute interval for up to 24 h. The relative intensities of substrate and product resonances were measured from their integrated intensities of spectra. Concentrations of the sulfide methyl singlet at 2.45 ppm was turned to the sulfoxide methyl singlet at 2.71 ppm with respect to the internal standard, 1,2-dichloroethane (3.73 ppm). Only very small quantities of sulfone was observed at 3.02 ppm after 24 h.

5.7. Electrochemistry

All electrochemical experiments were carried out under a solvent-saturated nitrogen atmosphere in deoxygenated, dry CH_3CN with 0.1 M $[NBu_4][ClO_4]$ as supporting electrolyte. Analyses used a 1 mm diameter platinum working electrode, a Pt wire auxiliary electrode and Ag/AgCl reference electrode separated from the working solution by a glass frit. A Pine WaveNow potentiostat was used for all electrochemical measurements. All potentials are referenced to the ferrocenium/ferrocene redox couple (Fc^+/Fc) added as an internal standard.

5.8. DFT calculations

All calculations were performed with the hybrid meta exchange–correlation functional M06 [59], as implemented by the Gaussian 09 program package [60]. The vanadium atom was described by Stuttgart-Dresden effective core potentials (ECP) and an SDD basis set [61], while a +6-31G(d') basis set was employed for the remaining atoms [62] Grimme's dispersion correction was included in all optimizations [63] The aryl methyl group present in the tridentate O,O,N ligand of complex **1** was replaced with a hydrogen.

The optimized structures represent a ground-state minimum based on the Hessian matrix that displayed only positive eigenvalues. The geometry-optimized structures presented here have been drawn with the JIMP2 molecular visualization and manipulation program [64].

CRediT authorship contribution statement

Md Kamal Hossain: Writing – review & editing, Writing – original draft, Investigation, Conceptualization. **Matti Haukka:** Investigation. **George C. Lisensky:** Writing – review & editing, Investigation. **Michael G. Richmond:** Writing – review & editing, Investigation. **Ebbe Nordlander:** Writing – review & editing, Supervision, Project administration, Funding acquisition, Conceptualization.

Declaration of competing interest

The authors declare that they have no known competing financial interests or personal relationships that could have appeared to influence the work reported in this paper.

Data availability

Data will be made available on request.

Acknowledgements

This research was supported by COST Action CM1003 *Biological oxidation reactions -mechanisms and design of* new catalysts. MGR thanks the Robert A. Welch Foundation (Grant B-1093) for funding. The DFT calculations were performed at the University of North Texas through CASCaM, which is an NSF-supported facility (CHE-1531468). M.K.H. gratefully acknowledge the European Commission for an Erasmus Mundus predoctoral fellowship. M.K.H also gratefully acknowledges the financial support from the Ministry of Science and Technology (Bangladesh) for part of the work. We thank Dr. Ari Lehtonen (University of Turku) for his assistance in preparing the initial draft of this work. We thank Dr. David A. Hrovat for the preparation of the spin density plots reported here. We thank Sofia Essén (Centre for Analysis and Synthesis, Lund University) for mass spectrometric measurements.

Appendix A. Supplementary data

^{51}V NMR figures, additional electrochemical figures, and DFT data are available in the Supplementary Information. CCDC 2090801-2090803 contains the supplementary crystallographic data for compounds **1**-**3**. These data can be obtained free of charge via http://www.ccdc.cam.ac.uk/conts/retrieving.html, or from the Cambridge Crystallographic Data Centre, 12 Union Road, Cambridge CB2 1EZ, UK; fax: (+44) 1223-336-033; or e-mail: deposit@ccdc.cam.ac.uk. Supplementary data to this article can be found online at https://doi.org/10.1016/j.poly.2024.117020.

References

[1] R.R. Langeslay, D.M. Kaphan, C.L. Marshall, P.C. Stair, A.P. Sattelberger, M. Delferro, Chem. Rev. 119 (2019) 2128–2191.
[2] (a) E. Amadio, R.D. Lorenzo, C. Zonta, G. Licini, Coord. Chem. Rev. 301–302 (2015) 147–162;
(b) V. Conte, A. Coletti, B. Floris, G. Licini, C. Zonta, Coord. Chem. Rev. 255 (2011) 2165–2177;
(c) V. Conte, B. Floris, Dalton Trans. 40 (2011) 1419–1436.
[3] (a) M. Kirihara, Coord. Chem. Rev. 255 (2011) 2281–2302;
(b) G. Licini, V. Conte, A. Coletti, M. Mba, C. Zonta, Coord. Chem. Rev. 255 (2011) 2345–2357.
[4] J.A.L. da Silva, J.J.R. Fraústo da Silva, A.J.L. Pombeiro, Coord. Chem. Rev. 255 (2011) 2232–2248.
[5] S.-S. Qian, Z. You, Y. Huo, Y.-T. Ye, X.-S. Cheng, H.-L. Zhu, J. Coord. Chem. 67 (2014) 2415–2424.
[6] M.M. Hänninen, A. Peuronen, P. Damlin, V. Tyystjärvi, H. Kivelä, A. Lehtonen, Dalton Trans. 43 (2014) 14022–14028.
[7] S. Groysman, I. Goldberg, Z. Goldschmidt, M. Kol, Inorg. Chem. 44 (2005) 5073–5080.
[8] G. Zhang, B.L. Scott, R. Wu, L.A.P. Silks, S.K. Hanson, Inorg Chem. 51 (2012) 7354–7361.
[9] M.R. Maurya, C. Haldar, A. Kumar, M.L. Kuznetsov, F. Avecilla, J.C. Pessoa, Dalton Trans. 42 (2013) (1962) 11941.
[10] P. Nayak, M. Nayak, K. Meena, S. Kar, New J. Chem. 46 (2022) 4634–4646.
[11] J.M. Brégeault, Dalton Trans. (2003) 3289–3302.
[12] S. Shylesh, M.J. Jia, W.R. Thiel, Eur. J. Inorg. Chem. (2010) 4395–4410.
[13] (a) E.N. Prilezhaeva, Russ. Chem. Rev. 69 (2000) 367–408;
(b) A. Mohammadinezhad, M.A. Nasseri, M. Salimi, RSC Adv. 4 (2014) 39870–39874.
[14] P. Salonen, A. Peuronen, A. Lehtonen, Inorg. Chem. Commun. 86 (2017) 165–167.
[15] M.K. Hossain, M. Haukka, G.C. Lisensky, A. Lehtonen, E. Nordlander, Inorg. Chim. Acta 487 (2019) 112–119.
[16] M. Sutradhar, L.M.D.R.S. Martins, M.F.C. Guedes da Silva, A.J.L. Pombeiro, Coord. Chem. Rev. 300–301 (2015) 200–239.
[17] S. Barroso, P. Adão, F. Madeira, M.T. Duarte, J.C. Pessoa, A.M. Martins, Inorg. Chem. 49 (2010) 7452–7463.
[18] M. Debnath, M. Dolai, K. Pal, S. Bhunya, A. Paul, H.M. Lee, M. Ali, Dalton Trans. 47 (2018) 2799–2809.
[19] S. Rayati, S. Zakavi, M. Koliaei, A. Wojtczak, A. Kozakiewicz, Inorg. Chem. Commun. 13 (2010) 203.
[20] M. Bagherzadeh, L. Tahsini, R. Latifi, L.K. Woo, Inorg. Chim. Acta 362 (2009) 3698.
[21] M. Bagherzadeh, L. Tahsini, R. Latifi, A. Ellern, L.K. Woo, Inorg. Chim. Acta 361 (2008) 2019.
[22] M. Bagherzadeh, R. Latifi, L. Tahsini, V. Amani, A. Ellern, L.K. Woo, Polyhedron 28 (2009) 2517.
[23] (a) H.H. Monfared, R. Bikas, P. Mayer, Inorg. Chim. Acta 363 (2010) 2574;
(b) H.H. Monfared, S. Kheirabadi, N.A. Lalami, P. Mayer, Polyhedron 30 (2011) 1375–1384.
[24] Y. Wang, M. Wang, Y. Wang, X. Wang, L. Wang, L. Sun, J. Catal. 273 (2010) 177–181.
[25] P. Mokhtari, G. Mohammadnezhad, Polyhedron 215 (2022) 115655.
[26] A. Zahirović, S. Hadžalić, A. Višanjevac, M. Fočak, B. Tüzün, D. Žilić, S. Roca, J. Jurec, A. Topčagić, I. Osmanković, J. Inorg. Biochem. 244 (2023) 112232.
[27] S.P. Dash, S. Majumder, A. Banerjee, M.F.N.N. Carvalho, P. Adão, J.C. Pessoa, K. Brzezinski, E. Garribba, H. Reuter, R. Dinda, Inorg. Chem. 55 (2016) 1165–1182.
[28] P. Adão, M.L. Kuznetsov, S. Barroso, A.M. Martins, F. Avecilla, J.C. Pessoa, Inorg. Chem. 51 (2012) 11430–11449.
[29] C. Ghosh, D. Patra, N. Bala, I. Majumder, N. Sepay, P. Mukhopadhyay, S. Das, R. Kundu, M.G.B. Drew, A.R. León, T. Ghosh, M. Pradhan, Biometals 35 (2022) 499–517.
[30] Q.-C. Zhou, T.-R. Wang, H. Li, L. Chen, J.-J. Xin, S. Guo, G.-H. Sheng, Z.-L. You, J. Inorg. Biochem. 196 (2019) 110680.
[31] S. Guo, N. Sun, Y. Ding, A. Li, Y. Jiang, W. Zhai, Z. Li, D. Qu, Z. You, Z. Anorg, Allg. Chem. 644 (2018) 1172–1176.
[32] Y. Huo, Y.-T. Ye, X.-S. Cheng, Z.-L. You, Inorg. Chem. Commun. 45 (2014) 131–134.
[33] M.A.S. Aslam, S. Mahmood, M. Shahid, A. Saeed, J. Iqbal, Eur. J. Med. Chem. 46 (2011) 5473–5479.
[34] N. Biswas, D. Patra, B. Mondal, M.G.B. Drew, T. Ghosh, J. Coord. Chem. 69 (2016) 318–329.
[35] N. Biswas, S. Bera, N. Sepay, T.K. Mukhopadhyay, K. Acharya, S. Ghosh, S. Acharyya, A.K. Biswas, M.G.B. Drew, T. Ghosh, New J. Chem. 43 (2019) 16714–16729.
[36] fish 0,punct]">L. Hernández, M.L. Araujo, W. Madden, E.D. Carpio, V. Lubes, G. Lubes, J. Inorg. Biochem. 229 (2022) 111712.
[37] P. Galloni, V. Conte, B. Floris, Coord. Chem. Rev. 301–302 (2015) 240–299.
[38] D. Patra, N. Biswas, B. Mondal, M.G.B. Drew, T. Ghosh, Polyhedron 48 (2012) 264–270.
[39] Y. Zhang, T. Yang, B.-Y. Zheng, M.-Y. Liu, N. Xing, Polyhedron 121 (2017) 123–129.
[40] A.-M. Li, J. Coord. Chem. 67 (2014) 2076–2085.
[41] K.-H. Yang, Transit. Met. Chem. 39 (2014) 469–475.
[42] D. Patra, N. Biswas, B. Kumari, P. Das, N. Sepay, S. Chatterjee, M.G.B. Drew, T. Ghosh, RSC Adv. 5 (2015) 92456–92472.
[43] D. Patra, N. Biswas, B. Mondal, P. Mitra, M.G.B. Drew, T. Ghosh, RSC Adv. 4 (2014) 22022–22034.
[44] D. Sadhukhan, M. Maiti, E. Zangrando, S. Pathan, S. Mitra, A. Patel, Polyhedron 69 (2014) 1–9.
[45] L. Suresh, J. Finnstad, K.W. Törnroos, E.L. Roux, Inorg. Chim. Acta 521 (2021) 120301.
[46] C. Hansch, A. Leo, R.W. Taft, Chem. Rev. 91 (1991) 165–195.
[47] E.C.E. Rosenthal, H. Cui, J. Koch, P.E. Gaede, M. Hummert, S. Dechert, Dalton Trans. (2005) 3108–3117.
[48] R. Dinda, P. Sengupta, S. Ghosh, T.C.W. Mak, Inorg. Chem. 41 (2002) 1684–1688.
[49] M.A. Nawi, T.L. Riechel, Inorg. Chem. 21 (1982) 2268–2271.
[50] The reported spin states for the radical cation and radical anion are based on the multiplicity ($2S + 1$), where S equals the spin quantum number. This value appears in the first subscript, while the second superscript represents the charge associated with the particular species. For example, the doublet species produced from oxidation of **A** is given by $^{2}\mathbf{A}^{1}$.
[51] F. Madeira, S. Barroso, S. Namorado, P.M. Reis, B. Royo, A.M. Martins, Inorg. Chim. Acta 383 (2012) 152–156.
[52] V. Conte, F. Fabbianesi, B. Floris, P. Galloni, D. Sordi, I.W.C.E. Arends, M. Bonchio, D. Rehder, D. Bogdal, Pure Appl. Chem. 81 (2009) 1265.
[53] V. Conte, B. Floris, Inorg. Chim. Acta 363 (2010) 1935–1946.
[54] Z. Otwinowski, W. Minor, in: C. W. Carter, J. Sweet, Methods Enzymol. 276 (1997) 307-326.
[55] Bruker, SADABS, Bruker AXS Inc., Madison, Wisconsin, USA, 2012.
[56] L. Palatinus, G. Chapuis, J. Appl. Crystallogr. 40 (2007) 786–790.
[57] G.M. Sheldrick, Acta Cryst. C 71 (2015) 3–8.
[58] (a) Y. Lei, C. Fu, J. Coord. Chem. 38 (2012) 65–70;
(b) R.M. Shakira, M.K.A. Wahab, N. Nordin, A. Ariffin, RSC Adv. 12 (2022) 17085–17095.
[59] Y. Zhao, D.G. Truhlar, Theor. Chem. Acc. 120 (2008) 215–241.
[60] M.J. Frisch, et al., Gaussian 09, Revision E.01, Gaussian Inc, Wallingford, CT, USA, 2009.
[61] D. Andrae, U. Haeussermann, M. Dolg, H. Stoll, H. Preuss, Theor. Chim. Acta 77 (1990) 123–141.
[62] (a) G.A. Petersson, A. Bennett, T.G. Tensfeldt, M.A. Al-Laham, W.A. Shirley, J. Mantzaris, J. Chem. Phys. 89 (1988) 2193–2218;
(b) G.A. Petersson, M.A. Al-Laham, J. Chem. Phys. 94 (1991) 6081–6090.
[63] S. Grimme, S. Ehrlich, L. Goerigk, J. Comp. Chem. 32 (2011) 1456–1465.
[64] (a) JIMP2, version 0.091, a free program for the visualization and manipulation of molecules: M.B. Hall, R.F. Fenske, Inorg. Chem. 11 (1972) 768-775; (b) J. Manson, C.E. Webster, M.B. Hall, Texas A&M University, College Station, TX, 2006, http://www.chem.tamu.edu/jimp2/index.html.